Excitation of Spin Waves in an In-Plane-Magnetized Ferromagnetic Nanowire Using Voltage-Controlled Magnetic Anisotropy

Roman Verba,[1,*] Mario Carpentieri,[2] Giovanni Finocchio,[3] Vasil Tiberkevich,[4] and Andrei Slavin[4]

[1]*Institute of Magnetism, Kyiv 03680, Ukraine*
[2]*Department of Electrical and Information Engineering, Politecnico di Bari, I-70125 Bari, Italy*
[3]*Department of Electronic Engineering, Industrial Chemistry and Engineering, University of Messina, I-98166 Messina, Italy*
[4]*Department of Physics, Oakland University, Rochester, Michigan 48309, USA*

(Received 21 February 2017; revised manuscript received 14 May 2017; published 16 June 2017)

It is demonstrated by analytical calculations and micromagnetic simulations that a microwave pumping by means of a voltage-controlled magnetic anisotropy (VCMA) could excite propagating spin waves in a ferromagnetic nanowire with in-plane static magnetization, and only the parametric excitation is possible. The efficiency of the parametric excitation is proportional to the out-of-plane component of the dynamic magnetization, and it is nonvanishing in the entire range of spin-wave wave vectors. This property ensures the excitation of spin waves in a wide frequency range (up to tens of gigahertz) using practically achievable amplitudes of the VCMA pumping. For a Fe/MgO nanowire, the threshold of parametric excitation of spin waves lies in the range 0.5–1 V/nm and only weakly depends on the nanowire width.

DOI: 10.1103/PhysRevApplied.7.064023

I. INTRODUCTION

The effect of voltage-controlled magnetic anisotropy (VCMA) manifests itself as a variation of the perpendicular magnetic anisotropy at the interface between a ferromagnetic metal and dielectric under the action of an electric field applied to the interface [1–3]. Similar to other magnetoelectric effects, e.g., in piezoelectric-piezomagnetic heterostructures, the effect of VCMA could provide an effective control of the magnetization in a ferromagnetic material with very low power consumption [4–6], much lower than using well-developed methods of magnetization control by magnetic field or electric current. The useful and convenient features of the VCMA effect, such as the technological simplicity of its application at nanoscale, high performance, and linearity as a function of the applied electric field [7–10] make VCMA one of the most attractive magnetoelectric effect for the application in spintronics and spin-wave (SW)-based signal processing, which currently attract significant research interest [11,12]. For example, the VCMA effect has been already proposed and tested for the application in magnetic recording [13,14], motion control of a domain wall [15,16], Skyrmions [17–19] and spin waves [20], and for the excitation of the ferromagnetic resonance [9,10,21].

In our previous works [22,23], we showed by both analytical calculations and micromagnetic simulations that microwave pumping by means of the VCMA could excite propagating SWs in an ultrathin ferromagnetic nanowire with an out-of-plane (OOP) static magnetization. In that case, VCMA pumping leads to the variation of the OOP component of the effective magnetic field, which is parallel to the static magnetization (so-called parallel pumping geometry [24]). Thus, in the case of OOP magnetization, the SWs cannot be excited in a common linear regime, when the frequencies of the driving signal and the SWs are the same. Instead, the parametric excitation—a well-known method of SW excitation where the frequency of pumping is 2 times larger than the frequency of the excited SW [24–26]—is possible.

For practical applications, it is very desirable to use devices without permanent magnetic field bias. It is known that the static state of unbiased ultrathin ferromagnetic films and nanowires depends often on their thickness—below a certain critical thickness, the static magnetization is OOP; above this thickness, in plane (IP) [27,28]. The critical value depends on the perpendicular surface magnetic anisotropy and the saturation magnetization and, typically, is on the order of 1 nm. Here, we show that, in the case of IP magnetization—as in the case of OOP magnetization—only the parametric excitation of SWs is possible. It is also shown that the parametric excitation in thicker IP-magnetized magnetic nanowires could be more efficient than in thinner OOP-magnetized nanowires, despite the fact that VCMA is a purely interface effect, and its efficiency therefore decreases with an increase of the nanowire thickness.

The relatively high efficiency of SW parametric excitation is not the only advantage of IP-magnetized thicker nanowires. Thicker nanowires are usually easier to fabricate, and they have better uniformity. Therefore, thicker IP-magnetized nanowires have a lower inhomogeneous

*Corresponding author.
verrv@ukr.net

broadening of the SW linewidth [29]. Because of the vanishing static demagnetization fields, in the case of IP magnetization, it is possible to achieve higher SW frequency at zero bias field. Also, the IP-magnetization geometry allows one to combine the VCMA-based SW excitation with the advantages of the interfacial Dzyaloshinskii-Moriya interaction (IDMI), which takes place in ferromagnetic films grown on a heavy-metal substrate [30,31]. The IDMI is known to result in a nonreciprocal SW propagation [30,32,33], and the largest nonreciprocity is achieved for the case of IP magnetization, while, for OOP static magnetization, nonreciprocity is absent [33,34]. Obviously, the nonreciprocity of the SW propagation could provide additional functionality of the SW signal-processing devices [35].

II. THEORY

The considered layered structure is shown in Fig. 1. It consists of a thin layer of a ferromagnetic metal (e.g., Fe) covered by a dielectric layer (e.g., MgO) formed as a nanowire of the width w_y. The metal excitation gate of the length L_g is placed on top of the nanowire. The static magnetization of the ferromagnetic layer lies in plane along the nanowire length (the x axis). Below, we use the material parameters of an Fe-MgO structure, which is often used in the VCMA experiments: saturation magnetization of $\mu_0 M_s = 2.1$ T, exchange length $\lambda_{\rm ex} = 3.4$ nm, perpendicular surface anisotropy energy $K_s = 1.36$ mJ/m^2, Gilbert damping $\alpha_G = 0.004$, nonuniform line broadening $\Delta\omega_{\rm nu} = 2\pi \times 230$ MHz, magnetoelectric coefficient $\beta_s = 100$ fJ/(V m) [28,29,36]. The thickness of the Fe layer is chosen to be $h = 1$ nm. The parameters used are the same as in Ref. [22], except for the thickness [the critical thickness, corresponding to the OOP-to-IP state transition for Fe/MgO film, is $h_{\rm cr} = 2K_s/(\mu_0 M_s^2) = 0.78$ nm, and it slightly increases for nanowires], which allows us to compare the excitation efficiencies in the OOP and IP geometries.

Magnetization dynamics in a nanowire is described by the Landau-Lifshitz equation for the magnetization vector $\boldsymbol{M}(\boldsymbol{r}, t)$:

$$\frac{\partial \boldsymbol{M}}{\partial t} = -\gamma \boldsymbol{M} \times \boldsymbol{B}_{\rm eff} - \frac{\gamma \alpha_G}{M_s} \boldsymbol{M} \times (\boldsymbol{M} \times \boldsymbol{B}_{\rm eff}), \qquad (1)$$

where γ is the gyromagnetic ratio, α_G is the Gilbert damping constant (strictly speaking, effective; see below),

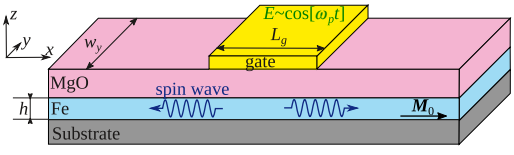

FIG. 1. A layout of the Fe-MgO nanowire with a VCMA excitation gate.

M_s is the saturation magnetization and $\boldsymbol{B}_{\rm eff}$ is the effective field consisting of external field (absent in our case), exchange, anisotropy, and magnetodipolar contributions. The variable microwave electric field $E(t) \sim \cos[\omega_p t]$ at the frequency ω_p, applied to the excitation gate, creates the variation of the perpendicular surface anisotropy $\Delta K_s = \beta E$. Corresponding variation of the effective field $\Delta \boldsymbol{B}_{\rm eff}$ can be found as a variational derivative of the anisotropy energy density $W_{\rm an} = -\Delta K_s M_z^2/(hM_s^2)$:

$$\Delta \boldsymbol{B}_{\rm eff}(t, \boldsymbol{r}) = -\frac{\delta}{\delta \boldsymbol{M}} \left(-\frac{\beta E M_z^2}{h M_s^2} \right) = \frac{2\beta E(t, \boldsymbol{r}) M_z(t, \boldsymbol{r})}{h M_s^2} \boldsymbol{e}_z. \qquad (2)$$

As one can see, the electrically driven component of the effective field is not orthogonal to the dynamic magnetization since both of them have nonzero z components, and, consequently, the effective field can linearly affect dynamic magnetization and SWs. This relation is in contrast to the case of OOP static magnetization, for which $\Delta \boldsymbol{B}_{\rm eff}$ [described by the same Eq. (2)] is parallel to the static magnetization. However, note, that $M_z(t)$ is the *dynamic* magnetization component having zero static value and varying at the frequency ω_k of the excited SW, if the excitation of SWs takes place. Thus, there are no terms in the expression for $\boldsymbol{B}_{\rm eff}$ proportional solely to the external force $E(t)$ and varying at the frequency of the external electric field. Consequently, the linear excitation of SWs in this geometry is impossible; nevertheless, the microwave VCMA-induced effective field is perpendicular to the static magnetization. It can be shown that the linear excitation of SWs becomes possible if the nanowire is magnetized at a finite angle to the surface $\theta_M \neq 0, \pi/2$ [10]. At the same time, if the variable electric field has the frequency component $\omega_p \approx 2\omega_k$, the effective magnetic field contains the *resonant* term at the SW frequency ω_k, and the *parametric* excitation of SWs may become possible.

To investigate SW dynamics, we use a standard expansion of magnetization as the sum of a static one and a series of SW modes: $\boldsymbol{M}(\boldsymbol{r},t) = M_s[\boldsymbol{e}_x + \sum_{n,k}(c_{n,k}\boldsymbol{m}_{n,k}e^{i(kx-\omega_{n,k}t)} + \text{c.c.})]$. SW modes are characterized by the wave vector $\boldsymbol{k} = k\boldsymbol{e}_x$ and quantization number $n = 0, 1, 2, \ldots$, which defines the SW mode profile $\boldsymbol{m}_{n,k} = \boldsymbol{m}_{n,k}(y)$ in the y direction (across the nanowire width). Substituting this representation into Eq. (1), one can obtain the following equation describing the dynamics of SW mode amplitude c_k [37]:

$$\frac{dc_k}{dt} + i\omega_k c_k + \Gamma_k c_k = \sum_{k'=-\infty}^{\infty} \frac{L_g}{l_x} V_{kk'} \tilde{b}_{k+k'} e^{-i\omega_p t} c_{k'}^*. \qquad (3)$$

Since pumping is uniform across the nanowire width, it does not lead to a coupling between modes with different width profiles (different n's), and the dynamics of SWs with a certain definite n is described by the same Eq. (3). For this

reason, we omit the index n in Eq. (3) and below. Value $\tilde{b}_k = L_g^{-1}\int b(x)e^{-ikx}dx$ in Eq. (3) is the Fourier image of a spatial profile of effective microwave pumping field $b(x) = 2\beta E(x)/(hM_s)$, l_x is the full length of the nanowire, and Γ_k is the SW damping rate which includes the Gilbert damping and the nonuniform SW line broadening. Equation (3) is absolutely the same as in the case of a parallel pumping [22,37], but the efficiency of the parametric interaction for the resonant case ($k' = -k$) is now equal to

$$|V_{k(-k)}| = |V_{kk}| = \gamma\frac{\langle|m_{k,z}|^2\rangle}{2A_k}. \tag{4}$$

Here, $A_k = i\langle \boldsymbol{m}_k^* \cdot \boldsymbol{e}_x \times \boldsymbol{m}_k\rangle$ is the norm of the SW mode [38], with the symbols $\langle\cdots\rangle$ mean averaging over the nanowire width. As one can see, the efficiency of the parametric excitation of SWs V_{kk} is proportional to the *out-of-plane magnetization component* $m_{k,z}$, and not to the difference of dynamic magnetization components $\langle|m_{k,y}|^2 - |m_{k,z}|^2\rangle$, as is the case for the usual parallel pumping (see, e.g., Ref. [37]). The appearance of such a dependence follows from Eq. (2). Indeed, $\Delta\boldsymbol{B}_{\text{eff}}$ is proportional to the z component of the dynamic magnetization and has only a z component, acting, thus, on the dynamical magnetization component m_z. In total, these factors result in the dependence $V_{kk} \sim |m_{k,z}|^2$. Equation (4) is one of the key results of this work, and it remains valid for any in-plane direction of static magnetization of the nanowire. We would like to note that parametric coupling with an efficiency like Eq. (4) cannot be realized by a microwave magnetic field and is intrinsic for anisotropy pumping.

For the lowest SW mode, which is uniform along the nanowire width, Eq. (4) is simplified to

$$|V_{kk}| = \frac{\gamma}{4}\frac{|m_{k,z}|}{|m_{k,y}|} = \frac{\gamma}{4}\sqrt{\frac{\gamma B + \omega_M(\lambda_{\text{ex}}^2k^2 + F_k^{(yy)})}{\gamma(B - B_{\text{an}}) + \omega_M(\lambda_{\text{ex}}^2k^2 + F_k^{(zz)})}}, \tag{5}$$

where B is the static internal field in the nanowire, $\hat{\boldsymbol{F}}_k$ is the dynamic demagnetization tensor [22] and $B_{\text{an}} = 2K_s/(M_sh)$ is the anisotropy field. The wave-number dependence of the parametric interaction efficiency V_{kk} for the lowest SW mode is shown in Fig. 2. The efficiency V_{kk} increases as the excited SW becomes shorter, and it saturates at the value $\gamma/4$ in the high-k range due to the circular polarization of the SWs [$|m_{k,y}| = |m_{k,z}|$, the limit $\lambda_{\text{ex}}k \gg 1$ in Eq. (5)] in this range of wave numbers. Thus, in the case of in-plane magnetization, there are no principal restrictions on the wave number of the excited SW. This property is in sharp contrast to the case of OOP magnetization, where the excitation efficiency V_{kk} could have a zero value at a certain wave number and vanishes completely at high wave numbers k [22]. For small values of the SW wave number k, the interaction efficiency is higher in narrower nanowires, as they have stronger in-plane demagnetization fields resulting in higher OOP dynamic magnetization (a larger $F_k^{(yy)}$ component).

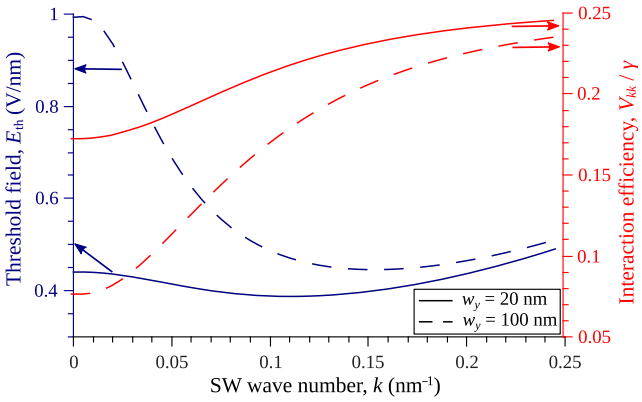

FIG. 2. Minimum parametric excitation threshold (the left axis) and efficiency of the VCMA-induced parametric interaction of spin waves (the right axis) as functions of the SW wave number for different widths of the ferromagnetic nanowire waveguide. Calculations are made for the lowest, uniform across the nanowire width, SW mode. Arrows show which curves belong to which axes.

It is well known that the parametric excitation of SWs is a threshold excitation—the SWs are excited only if the pumping strength overcomes a certain threshold [24]. The minimum possible excitation threshold is equal to $b_{\text{th}} = \Gamma_k/V_{kk}$ and is realized in the case of relatively large gate size, $L_g \gg \Gamma_k/v$ (where v is the SW group velocity), and when the pumping frequency is 2 times as large as the frequency of the excited SW, $\omega_p = 2\omega_k$ (this condition, along with the SW dispersion law, determines the wave number of the excited SW). The corresponding threshold amplitude of the microwave electric field $E_{\text{th}} = b_{\text{th}}M_sh/2\beta = \Gamma_kM_sh/(2\beta V_{kk})$ is shown in Fig. 2. It is clear that, in a relatively wide nanowire, it is easier to excite relatively short SWs, while the excitation of SWs with $k \to 0$ requires a higher amplitude of the electric-field pumping. In a relatively narrow nanowire, this difference becomes less and less pronounced. Consequently, it is desirable to use the narrow nanowire waveguides, having the width on the order of 10–20 nm, only when working with a small k, i.e., close to the ferromagnetic resonance (FMR) frequency. Away from the FMR (at a several-gigahertz distance) the difference in the nanowire width is practically insignificant, as, at $w_y > 30$ nm, the dependence of the parametric excitation threshold on the nanowire width saturates. This property also presents a contrast to the case of OOP magnetization, where the SW excitation threshold increases linearly up to $w_y \sim 70$–100 nm, so that the use of relatively narrow nanowires creates a significant advantage [22]. It should also be noted that the minimum values of characteristic threshold in the case of IP

magnetization are similar to that in the OOP case (about 0.5 V/nm). However, the range of the excited SW frequencies is much larger. For example, for a 20-nm-wide waveguide, the wave number range shown in Fig. 2, in which the threshold varies insignificantly, corresponds to the SW frequency range 6 GHz $< \omega_k/2\pi <$ 50 GHz. In a nanowire with the same geometry (except for the thickness) and OOP magnetization, the excitation threshold is smaller than 1 V/nm only in the range 5–9 GHz [22]. Thus, excitation of relatively high-frequency SWs is more efficient in the IP-magnetized case, which is a consequence of a different coupling of the pumping to SWs.

Of course, for practical applications, the excitation gate should have a finite length L_g, and the excited SWs should propagate from the gate to be processed and received by other gates. A finite gate length leads to an increase of the threshold, which is determined from the following implicit equation [23]:

$$\frac{\sqrt{(Vb)^2-(\Gamma-\alpha Vb)^2}}{\Gamma-\alpha Vb} = -\tan\frac{\sqrt{(Vb)^2-(\Gamma-\alpha Vb)^2}L_g}{v}. \tag{6}$$

Here, $V=|V_{kk}|$ and $\alpha=|\tilde{b}_{2k}/\tilde{b}_0|$ is the so-called measure of the pumping nonadiabaticity, which describes interaction of copropagating SWs with parametric pumping and is significant only when the pumping length L_g becomes comparable to or less than the SW wavelength [37]. For example, for the case of a rectangular pumping profile, $\alpha=|\mathrm{sinc}[kL_g]|$. The threshold increases from the minimum magnitude shown in Fig. 2, as the radiation losses $\Gamma_{\mathrm{rad}}=v/L_g$ increase in comparison to the natural damping rate Γ_k, which is equivalent to an increase of the SW propagation length $l_p=v/\Gamma_k$ compared to the gate length L_g. In the limiting case of a small gate length where $L_g \ll l_p$, the threshold is equal to $b_{\mathrm{th}}V_{kk}=\arccos(\alpha)(1+\alpha^2)^{-1/2}v/L_g$ [37]. For our parameters, the maximum propagation path is achieved for SWs of the wavelength $2\pi/k \sim 20$–30 nm, and it is about $l_p \approx 1$ μm.

III. MICROMAGNETIC SIMULATIONS

In order to verify the above-presented theoretical predictions, we perform micromagnetic simulations using the GPMagnet solver [39,40]. The nanowire-waveguide width is chosen to be $w_y=20$ nm, the gate length is $L_g=100$ nm, and the effective Gilbert constant is chosen to be $\alpha_G=0.033$, which approximately takes into account both the real Gilbert damping and the nonuniform SW line broadening in the studied range of SW frequencies. The thermal fluctuations corresponding to the temperature of $T=1$ K are also taken into account.

For these parameters, the FMR frequency, which is the lowest frequency in the SW spectrum, is $\omega_0/2\pi=6$ GHz. When the pumping frequency exceeds the double of the FMR frequency $\omega_p > 2\omega_0$, the propagating SWs can be excited at a certain threshold pumping amplitude, and the amplitude of excited SW increases monotonically above this threshold (Fig. 3). The wave number k of the parametrically excited SW is determined by the pumping frequency ($\omega_k=\omega_p/2$) and increases with an increase of the pumping frequency ω_p. Since the SW group velocity v also increases with an increase of the SW wave number k, the threshold of the SW excitation by a gate of a *finite length* increases with an increase of ω_p.

Our simulations also show that the parametric excitation of SWs is possible even when the pumping frequency ω_p is slightly lower than the double FMR frequency (the curve for 11.6 GHz in Fig. 3). However, in this case, the SW excitation is of a "subcritical" type—the amplitude of the excited SW has a large finite value at the threshold. The excitation in this frequency range becomes possible due to a nonlinear shift of the SW frequency, which is negative in our case—common for thin films and nanowires with IP static magnetization [24,41]. In this geometry, an increase of the SW amplitude leads to a decrease of the SW frequency $\omega_k(|c_k|^2)$, meaning that the parametric resonance condition $\omega_k(|c_k|^2)=\omega_p/2$ can be satisfied for $\omega_p < 2\omega_0$. The SW mode excited in such a case has an evanescent nonpropagating character and is localized in the region close to the excitation gate since it lies below the spectrum of linear propagating SWs.

The excitation thresholds observed in the simulations are $b_{\mathrm{th}}=58$, 78, and 90 mT for $\omega_p/2\pi=12.2$, 12.6, and 12.8 GHz, while Eq. (6) gives the threshold values of 55, 98, and 114 mT, respectively. The overestimation of the threshold for $\omega_p/2\pi=12.6$, 12.8 GHz in the analytical theory is related to the small theoretical values of the pumping nonadiabaticity $\alpha=|\mathrm{sinc}[kL_g]|$. In these cases,

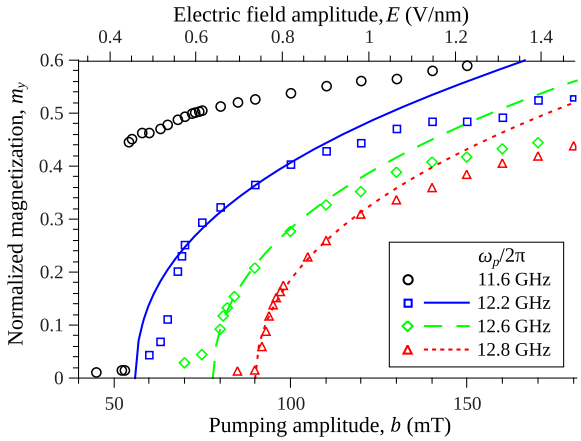

FIG. 3. Amplitudes of the excited SWs (normalized magnetization $m_y=M_y/M_s$ under the excitation-gate center) as functions of the pumping strength. Symbols, results of the micromagnetic simulations; lines, analytic theory.

$kL_g \simeq \pi/2$ and the theoretical value of the coefficient α is vanishingly small. In reality, the excited SW modes are not ideal plane waves, and they have a finite spread of wave numbers k. Thus, the effective nonadiabaticity parameter α cannot be zero, which results in a lower excitation threshold, as was shown in Ref. [37]. For the case $\omega_p/2\pi = 12.2$ GHz, the theoretical value of α is not small and pumping nonadiabaticity is not underestimated, resulting in a better theoretical prediction of the threshold.

Similar to the case of OOP magnetization, the amplitudes of parametrically excited SWs are determined by two mechanisms: (i) the "phase mechanism" related to the four-wave interaction between the excited SWs, and (ii) the amplitude dependence of the radiation losses existing due to the negative nonlinear frequency shift [23]. The simulated amplitudes of the excited SWs could be adequately described by the theory presented in Ref. [23] with the single fitting coefficients $C_\Sigma = 1.5$, 1.2, and 1.1 for $\omega_p/2\pi = 12.2$, 12.6, and 12.8 GHz, respectively (this fitting parameter depends on the degree of pumping localization and varies in the interval $1 < C_\Sigma < 2$ [23]). At high SW amplitudes, theoretical descriptions become less accurate since additional nonlinear SW interaction processes become important. It should be noted that, for the pumping frequency $\omega_p < 2\omega_0$, the analytical theory developed in Ref. [23] is not applicable and should be generalized.

IV. NOTES ON MULTIMODE NANOWIRES AND VCMA MATERIALS

All the above-presented calculations are made for the *lowest* SW mode, having a uniform profile along the nanowire width ($n = 0$). However, with an increase of the nanowire width, the higher SW width modes become closer in frequency to the uniform mode, and the parametric resonance condition $\omega_p = 2\omega_{n,k}$ could be satisfied for several SW width modes simultaneously [see, an example, Fig. 4(a)]. In such a case, it is not clear which SW mode would be excited in the waveguide. To answer this question, we plot the parametric interaction efficiency V_{kk} for different SW width modes in Fig. 4(b). As one can see, at a given frequency, V_{kk} has the largest value for the highest SW width mode since the spatially nonuniform width profile of a higher mode creates a larger dynamic demagnetization field along the y axis. This field results in a larger relative value of the z component of the dynamic magnetization, and, as shown above, the interaction efficiency V_{kk} is proportional to this z component of the dynamic magnetization. Also, at a given frequency, a higher SW mode has a lower k, and thus a lower SW group velocity $v \sim 2\omega_M \lambda_{ex}^2 k$. Thus, the highest mode has the lowest excitation threshold and will be excited by the parametric pumping. The other SW width modes may be excited only when the highest width mode reaches a sufficiently large amplitude [24]. It should be noted that the excitation of higher-order modes, having lower group velocity, limits the maximum propagation distance of the excited SWs, which is equal to the propagation length of the highest mode satisfying the conditions of parametric resonance. This property stimulates the use of narrow ferromagnetic nanowires in which a single-mode propagation regime exists in a wide range of frequencies.

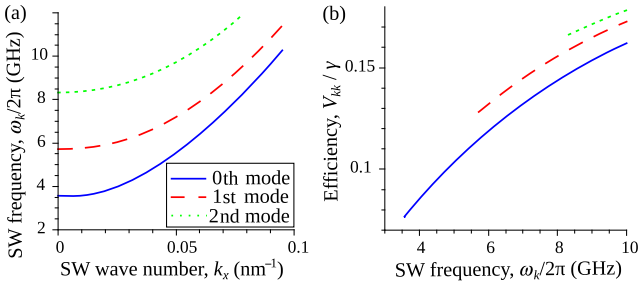

FIG. 4. (a) Spectrum of the three lowest SW width modes in a 100-nm-wide nanowire waveguide, and (b) efficiency of the parametric excitation of these modes as a function of their frequency. SW spectrum and mode structure in a finite-width waveguide are calculated using Ref. [42] and assuming "free" boundary conditions at the width edges of a nanowire.

Finally, we note that, in all of the above-presented calculations, we use the parameters of a typical VCMA material—a Fe-MgO multilayer. These calculations yield reasonable and experimentally reachable magnitude of the driving microwave electric fields needed for the parametric excitation of propagating SWs using the VCMA effect. Recent experimental and theoretical studies have found (or predicted) materials with substantially better VCMA characteristics, such as $SrTiO_3$/Fe bilayers, which have a 2 times larger magnetoelectric coefficient β than the Fe/MgO system [43], or a Cr/Fe/MgO multilayer having an almost 3 times larger β [44]. The use of these alternative materials should result in better characteristics of the SW processing devices based on parametric excitation of propagating spin waves through the VCMA effect.

V. SUMMARY

In this paper, we demonstrate that a microwave VCMA pumping can parametrically excite propagating SWs in an ultrathin ferromagnetic nanowire with in-plane static magnetization. The efficiency of the parametric interaction of propagating SWs by the VCMA pumping is proportional to the out-of-plane component of the dynamic magnetization of a nanowire. Such a type of parametric coupling is inherent to the case where the pumping is created by the time-dependent anisotropy of the magnetic film, and it cannot be realized by an application of a microwave magnetic field. The parametric interaction efficiency is nonvanishing in a wide range of SW wave numbers, including the region of short exchange-dominated SWs, where it tends to be $V_{kk} \to \gamma/4$. This useful property of the

VCMA-based parametric excitation of SWs in in-plane magnetized magnetic waveguides provides the practical method of excitation of short SWs, having sufficiently large group velocities for the development of energy-efficient signal-processing devices based on exchange-dominated short propagating SWs. The minimum excitation threshold is found to be about 0.5 V/nm in the Fe-MgO nanowire, and this threshold weakly depends on the nanowire width. At a large width of the nanowire, where the nanowire essentially becomes a multimode waveguide, the parametric VCMA pumping excites the highest SW width mode satisfying the parametric resonance condition.

ACKNOWLEDGMENTS

This work was supported in part by a grant from the Center for NanoFerroic Devices (CNFD) and the Nanoelectronics Research Initiative (NRI), by Grant No. EFMA-1641989 from the U.S. National Science Foundation, by a grant from DARPA, and by a contract from the U.S. Army TARDEC, RDECOM. R. V. acknowledges support from the Ministry of Education and Science of Ukraine, Project No. 0115U002716. The work of M. C. and G. F. was supported by the "Progetto Premiale—SIES Strategic Initiatives for the Environment and Security" and the executive program of scientific and technological cooperation between Italy and China (Code No. CN16GR09) funded by Ministero degli Affari Esteri e della Cooperazione Internazionale.

[1] M. Weisheit, S. Fähler, A. Marty, Y. Souche, C. Poinsignon, and D. Givord, Electric field-induced modification of magnetism in thin-film ferromagnets, Science **315**, 349 (2007).

[2] C.-G. Duan, J. P. Velev, R. F. Sabirianov, Z. Zhu, J. Chu, S. S. Jaswal, and E. Y. Tsymbal, Surface Magnetoelectric Effect in Ferromagnetic Metal Films, Phys. Rev. Lett. **101**, 137201 (2008).

[3] M. Endo, S. Kanai, S. Ikeda, F. Matsukura, and H. Ohno, Electric-field effects on thickness dependent magnetic anisotropy of sputtered $MgO/Co_{40}Fe_{40}B_{20}/Ta$ structures, Appl. Phys. Lett. **96**, 212503 (2010).

[4] M. Fiebig, Revival of the magnetoelectric effect, J. Phys. D **38**, R123 (2005).

[5] W.-Y. Tong, Y.-W. Fang, J. Cai, S.-J. Gong, and C.-G. Duan, Theoretical studies of all-electric spintronics utilizing multiferroic and magnetoelectric materials, Comput. Mater. Sci. **112, Part B**, 467 (2015).

[6] F. Matsukura, Y. Tokura, and H. Ohno, Control of magnetism by electric fields, Nat. Nanotechnol. **10**, 209 (2015).

[7] S.-S. Ha, N.-H. Kim, S. Lee, C.-Y. You, Y. Shiota, T. Maruyama, T. Nozaki, and Y. Suzuki, Voltage induced magnetic anisotropy change in ultrathin $Fe_{80}Co_{20}/MgO$ junctions with Brillouin light scattering, Appl. Phys. Lett. **96**, 142512 (2010).

[8] Y. Shiota, S. Murakami, F. Bonell, T. Nozaki, T. Shinjo, and Y. Suzuki, Quantitative evaluation of voltage-induced magnetic anisotropy change by magnetoresistance measurement, Appl. Phys. Express **4**, 043005 (2011).

[9] T. Nozaki, Y. Shiota, S. Miwa, S. Murakami, F. Bonell, S. Ishibashi, H. Kubota, K. Yakushiji, T. Saruya, A. Fukushima, S. Yuasa, T. Shinjo, and Y. Suzuki, Electric-field-induced ferromagnetic resonance excitation in an ultrathin ferromagnetic metal layer, Nat. Phys. **8**, 491 (2012).

[10] J. Zhu, J. A. Katine, G. E. Rowlands, Y.-J. Chen, Z. Duan, J. G. Alzate, P. Upadhyaya, J. Langer, P. K. Amiri, K. L. Wang, and I. N. Krivorotov, Voltage-Induced Ferromagnetic Resonance in Magnetic Tunnel Junctions, Phys. Rev. Lett. **108**, 197203 (2012).

[11] A. Khitun, M. Bao, and K. L. Wang, Magnonic logic circuits, J. Phys. D **43**, 264005 (2010).

[12] A. V. Chumak, V. I. Vasyuchka, A. A. Serga, and B. Hillebrands, Magnon spintronics, Nat. Phys. **11**, 453 (2015).

[13] Y. Shiota, T. Nozaki, F. Bonell, S. Murakami, T. Shinjo, and Y. Suzuki, Induction of coherent magnetization switching in a few atomic layers of FeCo using voltage pulses, Nat. Mater. **11**, 39 (2012).

[14] W.-G. Wang, M. Li, S. Hageman, and C. L. Chien, Electric-field-assisted switching in magnetic tunnel junctions, Nat. Mater. **11**, 64 (2012).

[15] A. Schellekens, A. van den Brink, J. Franken, H. Swagten, and B. Koopmans, Electric-field control of domain wall motion in perpendicularly magnetized materials, Nat. Commun. **3**, 847 (2012).

[16] U. Bauer, S. Emori, and G. S. D. Beach, Voltage-gated modulation of domain wall creep dynamics in an ultrathin metallic ferromagnet, Appl. Phys. Lett. **101**, 172403 (2012).

[17] X. Zhang, Y. Zhou, M. Ezawa, G. P. Zhao, and W. Zhao, Magnetic skyrmion transistor: skyrmion motion in a voltage-gated nanotrack, Sci. Rep. **5**, 11369 (2015).

[18] G. Finocchio, M. Ricci, R. Tomasello, A. Giordano, M. Lanuzza, V. Puliafito, P. Burrascano, B. Azzerboni, and M. Carpentieri, Skyrmion based microwave detectors and harvesting, Appl. Phys. Lett. **107**, 262401 (2015).

[19] F. H. Tung, G. W. Liang, and L. W. Siang, Gateable Skyrmion transport via field-induced potential barrier modulation, Sci. Rep. **6**, 21099 (2016).

[20] K. Nawaoka, Y. Shiota, S. Miwa, H. Tomita, E. Tamura, N. Mizuochi, T. Shinjo, and Y. Suzuki, Voltage modulation of propagating spin waves in Fe, J. Appl. Phys. **117**, 17A905 (2015).

[21] Y.-J. Chen, H. K. Lee, R. Verba, J. A. Katine, I. Barsukov, V. Tiberkevich, J. Q. Xiao, A. N. Slavin, and I. N. Krivorotov, Parametric resonance of magnetization excited by electric field, Nano Lett. **17**, 572 (2017).

[22] R. Verba, V. Tiberkevich, I. Krivorotov, and A. Slavin, Parametric Excitation of Spin Waves by Voltage-Controlled Magnetic Anisotropy, Phys. Rev. Applied **1**, 044006 (2014).

[23] R. Verba, M. Carpentieri, G. Finocchio, V. Tiberkevich, and A. Slavin, Excitation of propagating spin waves in ferromagnetic nanowires by microwave voltage-controlled magnetic anisotropy, Sci. Rep. **6**, 25018 (2016).

[24] V. S. L'vov, *Wave Turbulence Under Parametric Excitation* (Springer-Verlag, New York, 1994).

[25] T. Brächer, P. Pirro, F. Heussner, A. A. Serga, and B. Hillebrands, Localized parallel parametric generation of spin waves in a $Ni_{81}Fe_{19}$ waveguide by spatial variation of the pumping field, Appl. Phys. Lett. **104**, 092418 (2014).

[26] A. Capua, C. Rettner, and S. P. Parkin, Parametric Harmonic Generation as a Probe of Unconstrained Spin Magnetization Precession in the Shallow Barrier Limit, Phys. Rev. Lett. **116**, 047204 (2016).

[27] B. Heinrich and J. F. Cochran, Ultrathin metallic magnetic films: Magnetic anisotropies and exchange interactions, Adv. Phys. **42**, 523 (1993).

[28] H. X. Yang, M. Chshiev, B. Dieny, J. H. Lee, A. Manchon, and K. H. Shin, First-principles investigation of the very large perpendicular magnetic anisotropy at Fe|MgO and Co|MgO interfaces, Phys. Rev. B **84**, 054401 (2011).

[29] R. Urban, G. Woltersdorf, and B. Heinrich, Gilbert Damping in Single and Multilayer Ultrathin Films: Role of Interfaces in Nonlocal Spin Dynamics, Phys. Rev. Lett. **87**, 217204 (2001).

[30] L. Udvardi and L. Szunyogh, Chiral Asymmetry of the Spin-Wave Spectra in Ultrathin Magnetic Films, Phys. Rev. Lett. **102**, 207204 (2009).

[31] K.-S. Ryu, L. Thomas, S.-H. Yang, and S. Parkin, Chiral spin torque at magnetic domain walls, Nat. Nanotechnol. **8**, 527 (2013).

[32] R. L. Melcher, Linear Contribution to Spatial Dispersion in the Spin-Wave Spectrum of Ferromagnets, Phys. Rev. Lett. **30**, 125 (1973).

[33] V. L. Zhang, K. Di, H. S. Lim, S. C. Ng, M. H. Kuok, J. Yu, J. Yoon, X. Qiu, and H. Yang, In-plane angular dependence of the spin-wave nonreciprocity of an ultrathin film with Dzyaloshinskii-Moriya interaction, Appl. Phys. Lett. **107**, 022402 (2015).

[34] J.-H. Moon, S.-M. Seo, K.-J. Lee, K.-W. Kim, J. Ryu, H.-W. Lee, R. D. McMichael, and M. D. Stiles, Spin-wave propagation in the presence of interfacial Dzyaloshinskii-Moriya interaction, Phys. Rev. B **88**, 184404 (2013).

[35] R. Verba, V. Tiberkevich, and A. Slavin, Influence of interfacial Dzyaloshinskii-Moriya interaction on the parametric amplification of spin waves, Appl. Phys. Lett. **107**, 112402 (2015).

[36] M. K. Niranjan, C.-G. Duan, S. S. Jaswal, and E. Y. Tsymbal, Electric field effect on magnetization at the Fe/MgO(001) interface, Appl. Phys. Lett. **96**, 222504 (2010).

[37] G. A. Melkov, A. A. Serga, V. S. Tiberkevich, Y. V. Kobljanskij, and A. N. Slavin, Nonadiabatic interaction of a propagating wave packet with localized parametric pumping, Phys. Rev. E **63**, 066607 (2001).

[38] R. V. Verba, Spin waves in arrays of magnetic nanodots with magnetodipolar coupling, Ukr. J. Phys. **58**, 758 (2013).

[39] L. Lopez-Diaz, D. Aurelio, L. Torres, E. Martinez, M. A. Hernandez-Lopez, J. Gomez, O. Alejos, M. Carpentieri, G. Finocchio, and G. Consolo, Micromagnetic simulations using graphics processing units, J. Phys. D **45**, 323001 (2012).

[40] A. Giordano, G. Finocchio, L. Torres, M. Carpentieri, and B. Azzerboni, Semi-implicit integration scheme for Landau-Lifshitz-Gilbert-Slonczewski equation, J. Appl. Phys. **111**, 07D112 (2012).

[41] P. Krivosik and C. E. Patton, Hamiltonian formulation of nonlinear spin-wave dynamics: Theory and applications, Phys. Rev. B **82**, 184428 (2010).

[42] K. Y. Guslienko and A. N. Slavin, Magnetostatic Green's functions for the description of spin waves in finite rectangular magnetic dots and stripes, J. Magn. Magn. Mater. **323**, 2418 (2011).

[43] I. Kota and H. Imamura, Electric field effect on magnetic anisotropy in Fe-monolayer on $SrTiO_3$ and MgO insulating layer: A first-principles study, in *Proceedings of the 59th Annual Magnetism and Magnetic Materials (MMM) Conference, Honolulu*, 2014, p. CE-11, http://magnetism.org/doc/past_conferences/mmm_conference_59.pdf.

[44] T. Nozaki, A. Kozioł-Rachwał, W. Skowroński, V. Zayets, Y. Shiota, S. Tamaru, H. Kubota, A. Fukushima, S. Yuasa, and Y. Suzuki, Large Voltage-Induced Changes in the Perpendicular Magnetic Anisotropy of an MgO-Based Tunnel Junction with an Ultrathin Fe Layer, Phys. Rev. Applied **5**, 044006 (2016).